JACS
JOURNAL OF THE AMERICAN CHEMICAL SOCIETY

Article

pubs.acs.org/JACS

Surface Packing Determines the Redox Potential Shift of Cytochrome c Adsorbed on Gold

Laura Zanetti-Polzi,*[,†] Isabella Daidone,[‡] Carlo Augusto Bortolotti,[†,§] and Stefano Corni*[,†]

[†]Center S3, CNR NANO, Institute of Nanoscience, Via Campi 213/A, 41125, Modena, Italy
[‡]Department of Physical and Chemical Sciences, University of L'Aquila, via Vetoio (Coppito 1), 67010, L'Aquila, Italy
[§]Department of Life Sciences, University of Modena and Reggio Emilia, Via Campi 183, 41125, Modena, Italy

Supporting Information

ABSTRACT: Thermodynamic and dynamic properties of iso-1-*cytochrome c* covalently bound to a bare gold surface are here investigated by large scale atomistic simulations. The reduction potential of the protein for low and high surface concentrations is calculated showing a good agreement with experimental estimates. The origin of the dependence of the reduction potential on the surface concentration is investigated and is demonstrated to stem from the changing polarizability of the environment surrounding the protein, a mechanism reminiscent of crowding effects. Moreover, structural analyses are performed revealing relevant changes induced by the presence of the electrode on the dynamic properties of *cytochrome c*. In particular, one of the two cavities previously identified on the protein surface [Bortolotti et al. *J. Am. Chem. Soc.*, **2012**, *134*, 13670], and that reversibly open in *cytochrome c* freely diffusing in solution, is found to be deformed when the protein is adsorbed on gold. This modification exemplifies a mechanism that potentially leads to changes in the protein properties by surface-induced modification of its dynamical behavior.

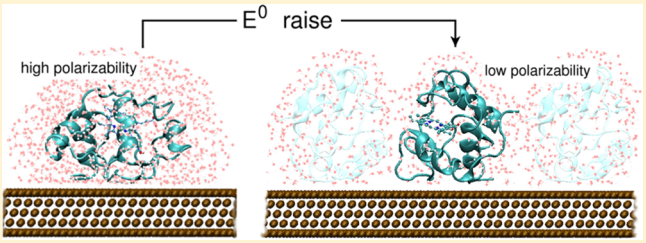

INTRODUCTION

The electrochemical investigation of redox-active proteins at electrodes is a challenging and highly interesting area of research, since these systems can be exploited for applications in biosensors,[1,2] bioelectronics,[3] and biofuel cells.[4,5] Despite many potential applications and the fundamental scientific interest, a deep understanding of the behavior of proteins immobilized on electrodes is still missing. An adequate insight into such mechanisms is, however, fundamental for enabling the optimization of the electrical communication between proteins and electrodes, which is a critical issue for the development of all the aforementioned applications.

When redox-active proteins are studied at electrodes, some fundamental difficulties have to be faced. For example, many proteins undergo denaturation when adsorbed at metal electrodes, resulting in dramatic changes of their electron transfer (ET) properties.[6] Even when the functionality is preserved upon surface tethering, the protein orientation toward the surface can severely influence the kinetic of the ET process.[7−9] Also, ET processes at the bioinorganic interface are poorly understood at the microscopic level, preventing the rational design of efficient biotechnological devices. The shortage of knowledge on bioinorganic interfaces is also due to the lack of suitable theoretical and computational methodologies: only recently, methodologies for bioinorganic interfaces are slowly becoming available.[10,11]

Cytochrome c (*cyt c*) is one of the most widely investigated ET proteins: it has been the focus of several experimental works and it has served as a paradigm for both biological redox activity and protein folding.[12−16] Computational methodologies were used as well to extensively investigate this protein,[17−23] also in interaction with bioinorganic interfaces.[20,22] Iso-1-*cytochrome c* from *Saccharomyces cerevisiae* (YCC) is of particular interest since it contains a single surface cysteine (Cys102) that can be exploited for specific tethering ensuring unique orientation of the protein. The electrochemistry and ET kinetics of YCC covalently bound to a bare gold electrode were studied,[24,25] obtaining results that point to a relevant role of the concentration of the proteins on the electrode surface. The importance of the orientation of the protein toward the electrode in affecting the ET kinetics was also highlighted by studying YCC and a series of its mutants[8] and in a recent computational study[26] the different ET behavior of YCC and one of such mutants was related to the flexibility of the portion of the protein where the anchoring Cys residue is placed.

In this work, a computational study of *cyt c* adsorbed on a gold surface is presented. In particular, by means of classical molecular dynamics (MD) simulations and a hybrid quantum mechanics/molecular mechanics (QM/MM) methodology, the perturbed matrix method (PMM), the redox potential of YCC adsorbed on a bare gold surface is calculated and, after validation by comparison with experimental results, insights are gained on the structural and dynamic determinants to the redox thermodynamics of the adsorbed molecule. In the PMM, in line with other QM/MM procedures,[27,28] a portion of the system is

Received: May 26, 2014
Published: August 1, 2014

   dx.doi.org/10.1021/ja505251a | *J. Am. Chem. Soc.* 2014, 136, 12929−12937

treated at the electronic level (the quantum center, QC), with the rest of the system described at a classical atomistic level exerting an electrostatic perturbation on the quantum-center electronic states. The method provides a reliable modeling of chemical processes in complex molecular systems, preserving both the quantum-chemical description of the chemical event and the configurational complexity of the overall atomic-molecular environment.[29−31] Indeed, the phase space sampling is provided by classical MD and thus a statistically relevant sampling of the quantum-center/environment configurations can be achieved, which is necessary for a proper description of functional properties in dynamical, complex systems, such as ET processes in proteins.

The PMM was recently used to calculate the redox potential of YCC freely diffusing in solution[32] obtaining results in excellent agreement with the experimental ones and highlighting the role of the heme hydration, as a consequence of the transient opening of solvent accessible cavities, in fine-tuning of the redox potential. Also in the present case, the calculation of the redox potential of YCC adsorbed on gold provides results in agreement with the experimental ones and gives an explanation to standing experimental data. Moreover, interesting differences in the dynamic behavior of YCC adsorbed on gold emerge, with possible fallout on the ET kinetics between the protein and the electrode.

METHODS

Molecular Dynamics Simulations. The gromos96 (53a6 version) force field parameters[33] are adopted for the protein and the heme in its reduced form. The atomic partial charges for the oxidized heme and the missing parameters describing axial and covalent links between the protein and the heme are taken from the literature.[32] The GolP force field,[34] that includes image charge effects,[35] is adopted for the polarizable Au(111) surface and to describe the interaction of YCC with the gold surface. Note that GolP parameters that describe the Lennard-Jones interaction between the gold and the protein atoms were optimized for the OPLS/AA force field while here the protein is parametrized with the gromos96 force field. In order to verify the viability of using the same parameters in the present case, the adsorption energy of a series of single amino acids on a Au(111) was calculated in vacuum using both the OPLS/AA and the gromos96 force fields parameters for the amino acids, obtaining consistent results. In the MD simulations and PMM calculations, it is assumed that the applied potential is that of zero charge; i.e., the gold electrode is neutral. Indeed, the potential of zero charge for an Au polycrystalline surface, as those used in the experiments, (+290 mV vs SHE[36]) is close to the reported redox potential of YCC (+268 mV vs SHE), thus guaranteeing that the calculations properly simulate the experimentally relevant electrode potential range. It has also to be noted that, as the aim of the present work is the calculation of the reduction potential, the approximation introduced by neglecting the electronic polarizability in the protein and water force fields is expected to be acceptable. The redox potential is indeed sensitive to the equilibrium polarizability of the environment, which is dominated by the reorientation of the polar groups in the protein rather than the electronic component.

The starting structures for the MD simulations of the single reduced and oxidized YCC on Au(111), hereafter called monomeric system, are extracted after 100 ns of previously performed[32] MD simulations of YCC in water in the reduced and oxidized ensemble, respectively. Such structures, properly rotated and translated in order to achieve the correct orientation of the protein toward the electrode, i.e., the direct interaction of the sulfur of Cys102 with the gold atoms, are then placed in a box ($6.43 \times 6.43 \times 6.10$ nm^3) filled with 5790 single point charge (SPC)[37] water molecules and 4 chloride ions. The dimension of the box is chosen in order to achieve a distance between the QC and the walls of the box similar to the one used in the previous simulation of YCC in water[32] (≈ 3 nm). Such a distance allows to have a water layer separating YCC to the next Au slab at least 2 times larger than the typical decay length of surface induced perturbation[38] assuring that the QC does not feel interactions with the next Au layer along z even mediated by water. A test simulation performed with a 0.5 nm higher box confirmed the independence of results upon the simulation box height, see Supporting Information for details. A schematic representation of the monomeric system is reported in Figure 1A.

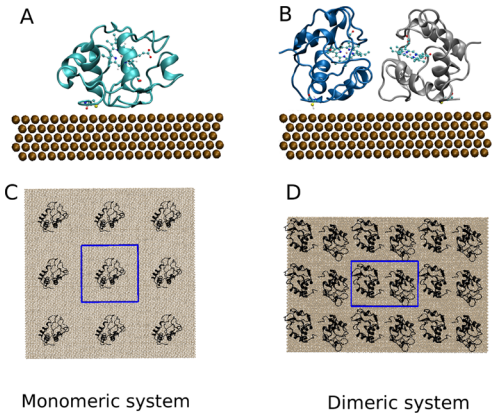

Figure 1. Representative snapshots of the monomeric system (A) and of the dimeric system (B). Residue Cys102 and the heme group of each monomer are highlighted in ball and sticks. (C,D) Schematic representation of the different electrode coverage in the monomeric (C) and in the dimeric (D) systems: the central box (highlighted with blue lines) is surrounded by its periodic images on the electrode plane. For the sake of clarity, water is not shown.

The starting structures for the MD simulations of the system in which two cytochromes are bound to Au(111) per each simulation cell, hereafter called dimeric system, are prepared as follows. The starting coordinates of the dimer are taken from the biological assembly of YCC (pdb code 1YCC) available in the Protein Data Bank. In the crystal unit cell of 1YCC various reciprocal orientations between the single asymmetric units are present. The two monomers belonging to the assembly are thus properly rotated and translated in order to achieve a conformation in which the heme groups of the two monomers face each other, as it is reasonable to assume that such a conformation maximizes the interaction between the two active sites, with possible fallout on the redox potential. Such a face-to-face conformation is thus properly oriented toward the gold electrode in order to allow the interaction between the sulfur atoms of Cys102 of the two proteins with the gold atoms. The dimer is then placed in a box ($6.09 \times 4.10 \times 6.50$ nm^3) filled with 3122 single point charge (SPC)[37] water molecules and 8 chloride ions. A smaller (in the directions parallel to the surface) box than the one used for the monomeric system is chosen in order to mimic, by exploiting the periodic boundary conditions in the MD simulation and in the PMM calculations (see Theory section), a crowded electrode in which the *cyt c* structures interact. The height of the box is increased with respect to the monomer's in order to maintain the previously mentioned z-distance of ≈ 3 nm between the QC and the wall of the box. In the dimeric system, as a consequence of the packing, the QC is indeed higher than in the monomeric one. A schematic representation of the dimeric system is reported in Figure 1B. In Figure 1D, a top view of the simulation box together with its periodic images on the electrode plane is provided, showing the high electrode coverage that characterizes the simulations of the dimeric system. In the simulation of the oxidation process in the dimeric system, it is assumed that the proteins are not oxidized all at the same instant, but rather that each protein is oxidized at a different time (as expected in the experiment, being a stochastic process) in the environment of the other proteins. In particular, a protein that changes from reduced to oxidized in the

dx.doi.org/10.1021/ja505251a | J. Am. Chem. Soc. 2014, 136, 12929−12937

presence of a protein that remains reduced is here considered. Thus, in the reduced ensemble the heme groups of both YCC monomers are in the reduced form and in the oxidized ensemble the heme group of one protein is in its oxidized form while the other is in its reduced form. In the experiment at high concentration[24] the voltammograms conform well to that of a layer with a single reduction potential; thus, a decisive role of the charge state of nearby proteins in determining the redox potential is not likely. It is also worth remarking that the choice of an all-reduced environment is the most conservative: on the basis of electrostatic considerations, nearby oxidized proteins would favor a further positive shift of the redox potential, and the experimental results would still be qualitatively reproduced.

After a solute optimization and a subsequent solvent relaxation, both the monomeric and the dimeric systems are gradually heated from 50 to 300 K using short MD simulations. For the dimeric system, a subsequent short pulling simulation with a harmonic potential is performed to achieve the proper distance between the Cys102 sulfur and the gold surface and the annealing procedure is then repeated. The trajectories are then propagated for 100 ns for the monomeric system and 180 ns for the dimeric system in the NVT ensemble with isokinetic temperature coupling[39] keeping the temperature constant at 300 K. Periodic boundary conditions are used, a nonbond pairlist cutoff of 9.0 Å is used and the long-range electrostatic interactions are treated with the particle mesh Ewald method.[40] The bond lengths are fixed[41] and a time step of 2 fs for numerical integration of the equations of motion is used. The simulations are performed with the GROMACS software package.[42] In order to compare the results for YCC on gold to the ones of YCC freely diffusing in water, all the adjustable parameters of the MD simulations (time step, cutoff radii, long-range electrostatic algorithm, etc.) are the same previously used for YCC in water.[32]

The first 10 and 80 ns are not used for the calculation of the reduction potential of the monomeric and dimeric systems, respectively. It is worth to remark that the dimeric system conformation is not directly extracted from a crystallographic structure but is manipulated in order to achieve the desired orientation between the monomers and toward the surface (see the discussion above). As confirmed also by the analysis performed on the convergence of the calculated reduction potentials during the simulations (see Supporting Information), the dimeric conformation needs a longer time than the monomeric one to reach an equilibrium state. For this reason, only the last 100 ns of the simulation of the dimeric system are used for the calculation of the redox potentials.

Quantum Chemical Calculations. A QC to be explicitly treated at the electronic level is necessary for the PMM/MD procedure to be applied (see Theory section). Here, the atoms of the prosthetic group and of the side chains of the axial ligands, i.e., His28 and Met90, are selected as QC. RMSD analysis ensures the stability of such a QC during the simulation and the absence of structural changes. Quantum chemical calculations were previously performed on the isolated QC for both redox states (with the iron(II) and iron(III))[32] and are here briefly summarized. The calculations were at the time-dependent density functional theory (TD-DFT) level with Becke's three parameters exchange and Lee, Yang and Parr correlation functionals (B3LYP). The atomic basis sets were as follows: (i) for the iron atom the LANL2DZ effective core potential for the inner electrons and a double Gaussian basis set of (5S,5P,5D)/[3S,3P,2D] quality for the valence electrons are used;[43] (ii) for the hydrogen, carbon, nitrogen, oxygen and sulfur atoms a standard 6-31+G(d)[44] Gaussian basis set was used. The first 12 unperturbed excited electronic (vertical) states were obtained on the ground state geometry using TD-DFT calculations. Although in general this level of theory might not provide a fully correct description of electronic excited states, in the case of the heme group it has already proved to represent a good compromise between computational cost and chemical accuracy.[45] All quantum chemical calculations were carried out using the Gaussian03 package.[46] More details on the quantum chemical calculations (including considerations on the choice of the size of the QC) can be found in the Supporting Information of ref 32.

THEORY

Perturbed Matrix Method. In PMM calculations,[47−51] similarly to other mixed quantum-classical procedures,[27,52,53] it is essential to predefine a portion of the system to be treated at the electronic level, the QC, with the rest of the system described at a classical atomistic level exerting a perturbation on the QC electronic states.

An orthonormal set of unperturbed electronic Hamiltonian ($\tilde{H}^0$) eigenfunctions (ϕ_j^0) are initially evaluated on the QC structure of interest. Indicating with $\mathcal{V}$ and $\boldsymbol{E}$ the perturbing electric potential and field, respectively, exerted by the environment on the QC (typically obtained by the environment atomic charge distribution and evaluated in the QC center of mass), the perturbed electronic Hamiltonian ($\tilde{H}$) for each QC-environment configuration (as generated by the MD simulation) can be constructed:

$$\tilde{H} \simeq \tilde{H}^0 + \tilde{I} q_T \mathcal{V} + \tilde{Z}_1 + \Delta V \tilde{I} \tag{1}$$

$$[\tilde{Z}_1]_{j,j'} = -\boldsymbol{E}\cdot\langle \phi_j^0 | \hat{\boldsymbol{\mu}} | \phi_{j'}^0 \rangle \tag{2}$$

where q_T, $\hat{\boldsymbol{\mu}}$ and ϕ_j^0 are the QC total charge, dipole operator and unperturbed electronic eigenfunctions, respectively, ΔV approximates all the higher order terms as a simple short-range potential, $\tilde{I}$ is the identity matrix and the angled brackets indicate integration over the electronic coordinates. The diagonalization of $\tilde{H}$ provides a set of eigenvectors and eigenvalues representing the QC perturbed electronic eigenstates and energies. When only the perturbed electronic ground-state energy shift is needed for the calculation of the property of interest with no atomic positional changes involved, as in the case of the calculation of the reduction potential, ΔV can be disregarded.

The QC for *cyt c* includes the atoms of the prosthetic group and of the side chains of the axial ligands, i.e., one histidine and one methionine. The solvent, the gold electrode and the rest of the protein define therefore the perturbing environment at each configuration generated by MD simulations. As mentioned in the Methods section, in the dimeric system a protein that changes from reduced to oxidized in the presence of a protein that remains reduced is considered. Thus, in the PMM calculation the heme group (with its two ligands) of only one protein (hereafter termed as active QC-containing protein) constitutes the QC of the system. Moreover, to mimic the electrostatic effect on such a QC of a series of coadsorbed proteins, the first and second nearest-neighbors periodic images of the central box on the electrode plane are explicitly included in the PMM calculation. In other words, the central box is replicated in the x and y directions resulting in a layer of 18 tightly packed proteins: 1 containing the active-QC, 1 is the other protein in the original cell, 8 from the nearest-neighbors cells, 8 from the second nearest-neighbors cells (see Figure 1D). All these proteins are part of the perturbing environment together with gold, ions and water. Beside mimicking the high surface concentration condition, the use of the periodic images of the central box during the calculations implies also that two possible reciprocal orientation between the proteins are explicitly considered. In fact, defining as "back" the side of the protein opposite to the heme, and "face" the side where the heme stays, each protein has one face-to-face and one back-to-back nearest-neighbor, see Figure 1D.

Calculation of the Redox Potentials. The (Helmholtz) free energy change ΔA^0 associated with the $Fe^{3+} + e^- \rightarrow Fe^{2+}$

dx.doi.org/10.1021/ja505251a | J. Am. Chem. Soc. 2014, 136, 12929−12937

semireaction (related to the reduction potential via $E^0 = -\Delta A^0/F$, with F the Faraday constant) is calculated using the following equation:[54]

$$\Delta A^0 = -k_B T \ln\langle e^{-\beta\Delta\mathcal{U}_{ox\to red}}\rangle_{ox} = k_B T \ln\langle e^{-\beta\Delta\mathcal{U}_{red\to ox}}\rangle_{red}$$
$$\approx -k_B T \ln\langle e^{-\beta\Delta\varepsilon_{ox\to red}}\rangle_{ox} = k_B T \ln\langle e^{-\beta\Delta\varepsilon_{red\to ox}}\rangle_{red} \quad (3)$$

In the above equation $\Delta\mathcal{U}_{ox\to red(red\to ox)}$ is the whole system energy change upon reduction (oxidation), $\Delta\varepsilon_{ox\to red(red\to ox)} = \varepsilon_{red} - \varepsilon_{ox}(\varepsilon_{ox} - \varepsilon_{red})$, with ε_{red} and ε_{ox} representing the perturbed ground-state electronic energy of the red (reduced) and ox (oxidized) chemical states, respectively, and use was made of the approximation $\Delta\mathcal{U}_{ox\to red(red\to ox)} \approx \Delta\varepsilon_{ox\to red(red\to ox)}$; i.e., the environment internal energy change associated with the QC reduction is disregarded being exactly zero within the present description.[51] ε_{red} and ε_{ox} are evaluated at each MD frame via the PMM approach described in the Theory section and averaging is performed in either the oxidized or reduced ensemble as indicated by the subscript of the angle brackets.

Although eq 3 is based on an exact relation in principle, given the sampling problems of finite-time simulations, the best estimate of the reduction free energy is obtained by averaging the values provided by the reduced and oxidized ensembles:[18]

$$\Delta A^0 = \frac{-k_B T \ln\langle e^{-\beta\Delta\varepsilon_{ox\to red}}\rangle_{ox} + k_B T \ln\langle e^{-\beta\Delta\varepsilon_{red\to ox}}\rangle_{red}}{2} \quad (4)$$

The redox potentials have been also calculated within the linear response approximation[18] quantitatively providing the same picture.

RESULTS AND DISCUSSION

Analysis of the Redox Potential Shift upon YCC Adsorption. In a previous work,[32] the redox potential of YCC in solution was calculated applying the PMM methodology and resulting in excellent agreement with the experimental estimate. Here, the same methodology (briefly outlined in the Theory section) is used to calculate the redox potential of YCC covalently bound to a gold surface.

Experimentally, the redox potential of YCC adsorbed on a gold electrode is 110 mV more positive than that for the freely diffusing protein in solution.[24] Such an increase has been suggested to be a consequence of the packing of the proteins on the electrode surface: the result is indeed obtained with a coverage of 90% of the electrode surface and is remarkably different from the value obtained with a coverage of 5−40% (where the reduction potential is essentially equal to the one of the freely diffusing protein).[25] In particular, the increase of the reduction potential has been hypothesized to be a consequence of the strong electrostatic repulsion among the positively charged proteins densely packed on the electrode surface.[24] However, the experimental shift of the redox potential due to the high coverage of the electrode surface could also depend on the different dielectric environment constituted by the proteins that surround the one that undergoes the redox process. Thanks to the approach here used, it is possible to discriminate between these two possible scenarios.

In order to verify the effect of the surface concentration on the variation of the redox potential of YCC immobilized on gold and to give insight into the molecular mechanism underlying the experimental results, calculations are performed for two systems that model the low and high density conditions. The former is a single surface-bound cytochrome in a large simulation box (monomeric system), the latter consists of two surface-bound cytochromes (dimeric system) in a simulation box that yield high density via the periodic boundary conditions (see Methods section). The different coverage of the electrode surface in the two simulated systems can be observed in Figure 1C,D.

The redox potential is obtained, according to eq 4, by calculating the energy difference $\Delta\varepsilon_{ox\to red}$ and $\Delta\varepsilon_{red\to ox}$ in the oxidized and reduced ensemble, respectively, between the perturbed ground-state electronic energy of the reduced (ε_{red}) and oxidized (ε_{ox}) chemical states of the QC. In Figure 2 the energy difference $\Delta\varepsilon$ is reported as a function of time both for the monomeric (Figure 2A,B) and the dimeric (Figure 2C,D) systems in the two simulation ensembles (reduced and oxidized). The calculated redox potentials are summarized in Table 1.

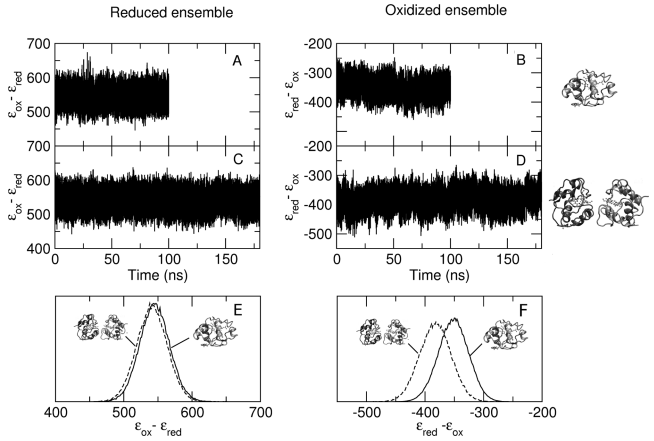

Figure 2. (A−D) Time course of the difference between the perturbed ground-state electronic energy of the reduced and oxidized chemical states calculated from the reduced (A,C) and oxidized (B,D) YCC simulations of the monomeric (A,B) and dimeric (C,D) system. (E,F) Normalized distribution of the perturbed ground-state energy difference for the monomeric (continuous line) and dimeric (dashed line) systems in the reduced (E) and oxidized (F) ensembles. Energy values in kJ/mol.

The calculated redox potential of the monomeric system is 4.698 ± 0.041 V (i.e., +278 ± 41 mV vs SHE), very close to the calculated value for the freely diffusing molecule (4.720 ± 0.014 V, +300 ± 14 mV vs SHE)[32] and in agreement with the experimental value of 4.688 V (+268 mV vs SHE) obtained with a low coverage of the electrode.[25] Please note that, in order to compare calculated absolute E^0 values to experimental ones, the IUPAC recommended value of 4.420 V for the standard hydrogen electrode (SHE) was added to the latter. The calculated redox potential of the dimeric system is 4.838 ± 0.031 V (+418 ± 31 mV vs SHE), i.e., 118 mV higher than the one for the freely diffusing protein in solution, in very good agreement with the experimentally observed raise of 110 mV.[24] Note that the experimental redox potentials are obtained from measures at nonzero ionic strength while the computed values of E^0 are evaluated at null ionic strength. The difference in the ionic strength should not affect the comparison between the experimental (+110 mV) and calculated (+118 mV) shifts. Indeed, the ionic strength could affect the redox potential of

dx.doi.org/10.1021/ja505251a | J. Am. Chem. Soc. 2014, 136, 12929−12937

Table 1. Reduction Potentials of YCC[a]

	freely diffusing YCC	monomeric system	dimeric system
$E^0_{red\ ens}$ (V)	4.868 ± 0.016(0.448)[b]	4.910 ± 0.037(0.490)	4.875 ± 0.023(0.455)
$E^0_{ox\ ens}$ (V)	4.573 ± 0.013(0.153)[b]	4.486 ± 0.046(0.066)	4.801 ± 0.040(0.381)
$\langle E^0 \rangle$ (V)	4.720 ± 0.014(0.300)[b]	4.698 ± 0.041(0.278)	4.838 ± 0.031(0.418)
Experimental E^0 (V)	4.680(0.260)[c]	4.688(0.268)[d]	4.790(0.370)[e]

[a] $E^0_{red\ ens}$ and $E^0_{ox\ ens}$ refer to the reduction potentials calculated from the two ensembles, respectively. $\langle E^0 \rangle$ is the average of such values and is the result to be compared with the experimental E^0. The values reported in parentheses are relative to the SHE. [b] See ref.[32] [c] See ref.[24] [d] Obtained with low electrode coverage; see ref.[25] [e] Obtained with high electrode coverage; see ref.[24]

YCC on gold (i) via Debye–Hückel effect and (ii) by determining the extent of screening of the redox center from the electrode charge. In solution only (i) is relevant and it is expected that such Debye–Hückel effects (small anyway[24]) cancel out in the shift. Concerning (ii), as long as the ionic strength is high enough to ensure this screening, no large dependence is expected. In the present case, the closeness of the electrode potential of zero charge and E^0 noted in the Methods section makes the electrode charge small in the relevant applied potential range, and thus a particularly limited effect of the ionic strength is reasonable. Indeed, the same reduction potential has been experimentally obtained by Heering et al.[25] with different ionic strengths. The comparison between the calculated and the experimental potentials is thus also meaningful and their agreement is good (see Table 1). The results calculated here reproduce the experimental finding of a relevant effect of the electrode coverage on the redox potential of YCC bound to gold.

It can be observed that the raise of the redox potential has to be ascribed solely to the contribution of the oxidized ensemble (see Table 1 and Figure 2E,F). Indeed, the distribution of $\Delta\varepsilon$ shows that in the reduced ensemble the energy difference is almost the same in the dimeric and in the monomeric system, while in the oxidized ensemble the absolute value of $\Delta\varepsilon$ is higher in the dimeric system than in the monomeric one. In other words, the oxidized state is destabilized in the oxidized ensemble simulation of the dimeric system with respect to the monomeric one.

As mentioned in the Theory section, the results reported arise from the contribution of two reciprocal orientations between the proteins: the face-to-face and the back-to-back. However, another limit reciprocal orientation between the two molecules is possible, i.e., the face-to-back one. To complete the analysis, a test is performed with this orientation. Such a test, reported in the Supporting Information, provides a picture similar to what discussed so far.

In order to investigate such a destabilization, the electrostatic potential acting on the QC is analyzed, providing the results shown in Figure 3, in which the distributions of the electrostatic potential exerted on the QC by the various components of the perturbing environment are reported in both the reduced and oxidized ensemble. In particular, the following components are analyzed: (i) the electrostatic potential due to water, gold and ions, (ii) the electrostatic potential due to the protein that contains the active QC, and (iii) in the case of the dimeric system, the electrostatic potential due to the surrounding proteins. From the electrostatic potential distributions it is evident that the behavior of the monomeric and dimeric system upon oxidation is considerably different. In the monomeric system, the electrostatic potential distribution due to the protein and due to the rest of the environment (water, ions and gold) are both shifted upon oxidation toward smaller values, as

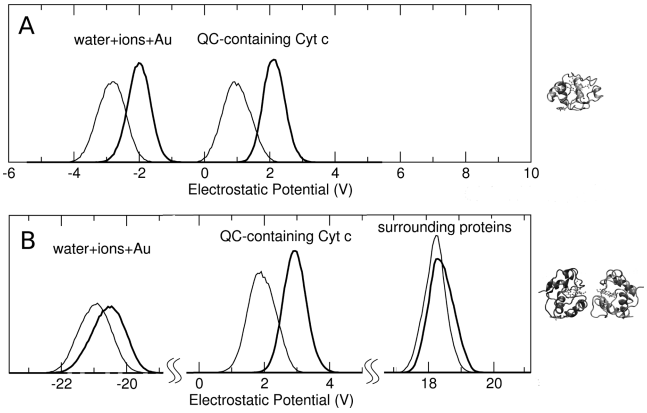

Figure 3. Normalized distribution of the electrostatic potential exerted on the active site by water, gold and ions, by the active QC-containing YCC and, for the dimeric system, by the proteins surrounding the active QC-containing one obtained from the simulations in the reduced (thick lines) and oxidized (thin lines) ensembles of the monomeric (A) and dimeric (B) ensembles.

a consequence of the positively charged quantum center in the oxidized state. The shift of the distribution of the electrostatic potential exerted by water, gold and ions is almost entirely due to the water contribution, thus implying that the solvent around the oxidized protein is more efficiently interacting with the protein, i.e., more polarized. Similarly, the shift of the electrostatic potential due to the protein depends on the rearrangement of the atomic positions in order to optimize the electrostatic interaction with the charged QC.

In the dimeric system, a shift similar to the one in the monomeric system can be observed for the active QC-containing protein. Yet, in this case, the other components of the electrostatic potential show a different behavior. It can be observed indeed that both the electrostatic potential due to the other proteins that compose the system and the one due to water, ions and gold are only slightly shifted upon oxidation. When the active QC-containing protein is surrounded by other proteins the effect of the charged QC on the water molecules is obviously less intense, as many water molecules have been removed by the surrounding proteins and the remaining ones are far enough from the QC not to be significantly polarized. The atoms of the proteins surrounding the central one are not as prone as water molecules to be polarized by the charged QC, as the protein scaffold limits their movement.

Therefore, the inability of the environment that surrounds the QC to rearrange consequently to the change of charge status of the active site is at the origin of the destabilization of the oxidized state in the dimeric system and thus at the origin of the change in the redox potential experimentally observed. Interpreting this result in terms of effective dielectric constant of protein and water, it can be said that the shift of the redox

dx.doi.org/10.1021/ja505251a | J. Am. Chem. Soc. 2014, 136, 12929–12937

potential is due to the low-dielectric constant environment of the protein layer compared to water.

Structural Changes upon Adsorption. As previously mentioned, it is well-known that when a protein is adsorbed on an inorganic surface the retain of its structure and functionality is fundamental for biotechnological applications. The structural and dynamic properties of YCC adsorbed on a gold electrode are thus analyzed both for the monomeric and the dimeric system and compared to the ones of the freely diffusing protein. In Figure 4 the percentage of residues in each secondary

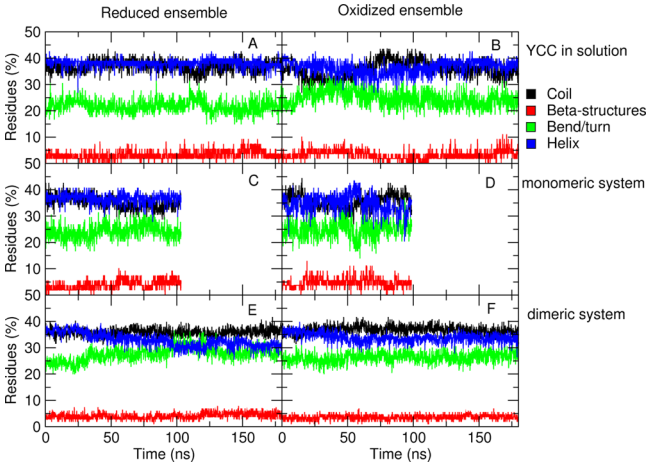

Figure 4. Time evolution of the secondary structure of YCC in the reduced (left panels) and oxidized (right panels) simulation ensembles in solution (A,B), in the monomeric system (C,D) and in the dimeric system (E,F). Color code: black line, random coil; red line, beta structures; green line, bends and turns; blue line, helical conformations.

structure state is reported as a function of time in both simulation ensembles for YCC freely diffusing in solution and adsorbed on gold (both in the monomeric and in the dimeric system). It can be seen from the Figure that the overall secondary structure of YCC is very stable in solution (Figure 4A,B) and is well retained when the protein is adsorbed on gold, both in the monomeric system (Figure 4C,D) and in the dimeric one (Figure 4E,F), in agreement with previous simulation with a different force field.[26] The only notable feature is the slight loss of helical conformation (≈10%) in the dimeric system, both in the oxidized and in the reduced ensemble, likely due to the interaction between the two proteins. Such a loss arises from the deformation of the first helix that follows the N-terminal tail of the non active QC-containing protein. The residue-specific dssp analysis of the secondary structure can be found in the Supporting Information and confirms that no relevant conformational transition is induced by the adsorption of the protein on the surface.

However, the presence of the gold electrode induces a deformation of the shape of the protein, that becomes slightly flattened when adsorbed on gold. This can be observed by calculating as a function of time the semiaxes a, b, c of the ellipsoid that best approximates the protein shape.[55] In particular, the ratio $\xi = a/(b^2 + c^2)^{1/2}$, where a is the minor semiaxis, provides the degree of "flattening" of the protein (note that for a sphere $\xi = 1/\sqrt{2} \approx 0.71$ while for a disc $\xi = 0$). In Figure 5, the distribution of the ratio ξ is reported for YCC freely diffusing in solution, for the monomeric system and for

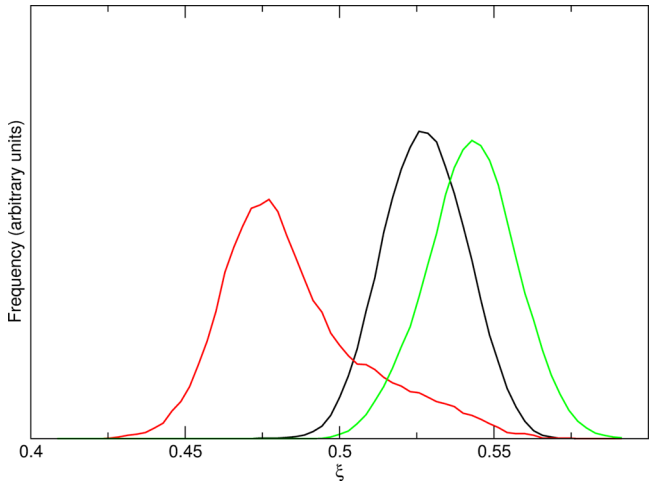

Figure 5. Distribution of the parameter ξ of YCC in solution (black line), of the monomeric system (red line) and of the dimeric system (green line). A higher ξ corresponds to a more spherical shape, while a lower ξ to a more flattened shape. Note that the ξ distribution reported is obtained from the mean value of the ξ parameter calculated in the reduced and oxidized simulation ensembles.

the dimeric one. Interestingly, it can be observed that the adsorption on the electrode induces a clear flattening of YCC in the monomeric system while the ξ of the dimeric system is essentially unchanged with respect to the one of the protein in solution. The close coadsorption of the proteins on the surface is thus able to prevent the deformation of the proteins' shape.

Dynamic Behavior of the Cavities on the Protein Surface. A relevant dynamic feature previously observed in the MD trajectory of YCC in solution is the reversible opening of two cavities in the protein surface, each facing one of the heme propionates. Opening of the cavities allows water access into the protein matrix and provides direct access of water molecules to the heme propionates.[32] The access of water to the propionates determines, for YCC freely diffusing in solution, a positive shift of the reduction potential of ≈45−50 mV. The hydration state of the heme propionates is thus related to small but non-negligible variations of the redox potential. Each cavity is defined by two groups of residues belonging to loops placed on opposite sides and facing each other. According to the definition previously exploited,[32] one cavity is defined by residues 49−52 on one side and 76−79 on the other (cavity A) and provides direct access to the so-called outer propionate (propionate-6). The other cavity (cavity B) is defined by residues 31−35 on one side and 41−43 on the other and allows solvent molecules to enter the protein matrix pointing directly at the inner propionate-7.

The presence of these cavities and their dynamic behavior during the simulated trajectories of the dimeric and monomeric systems are investigated in order to highlight possible relevant changes induced by the presence of the gold surface. The same definition of the open and closed cavities used for YCC in solution is applied also to the present case: the opening and closing of cavity A is described by plotting the time dependence of the distance between the C_α atoms of residues 50 and 77, lying on opposite sides of the cavity mouth. The cavity is considered open when the distance is higher than 0.62 nm. Similarly, the behavior of cavity B is investigated by monitoring the distance between the C_α atoms of residues 31 and 43, also sitting at opposites sides of the mouth of the cavity, which is

dx.doi.org/10.1021/ja505251a | J. Am. Chem. Soc. 2014, 136, 12929−12937

considered open when the distance between the two C_α atoms is higher than 0.65 nm. In Figure 6, such distances are plotted

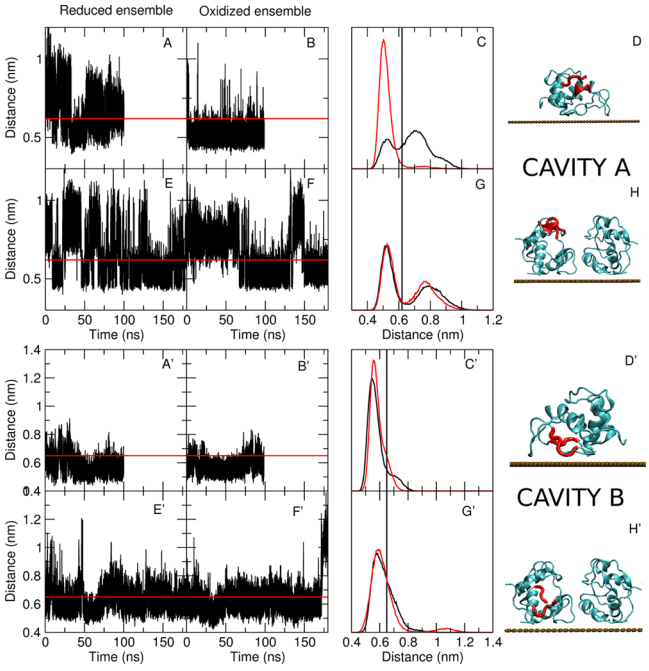

Figure 6. Panels A−H refer to cavity A and panels A′−H′ refer to cavity B. (A,B,E,F,A′,B′,E′,F′) Time course of the C_α distance for the monomeric system (A,B,A′,B′) and for the dimeric system (E,F,E′,F′) in the reduced (A,E,A′,E′) and oxidized (B,F,B′,F′) MD simulation ensembles. The red line highlights the cutoff distance (0.62 nm and 0.65 nm for cavities A and B, respectively) that was chosen as a reference to discern between the closed and the open conformation.[32] (C,G,C′,G′) Normalized distribution of the C_α distance for the monomeric system (C,C′) and dimeric system (G,G′) in the reduced (black line) and oxidized (red line) simulation ensembles. The vertical black line highlights the cutoff distance chosen as a reference to discern between the closed and the open conformation. (D,H,D′,H′) Representative snapshot showing the position of the cavities in the monomeric system (D,D′) and in the dimeric system (H,H′). The residues that define the two cavities are highlighted in red.

both in the reduced and in the oxidized simulation ensemble for the monomeric and the dimeric system. In the upper box of Figure 6 cavity A is analyzed (Figure 6A−H). In panels A, B, E, F, the time evolution of the distance between the previously defined C_α atoms is reported, while in panels C and G the distribution of such distances is plotted, in order to show (when present) the bimodal trend associated with the reversible opening and closing of the cavity. Moreover, in panels D and H, a representative snapshot of the protein is provided in which the residues that define the cavity are highlighted. In the lower box of Figure 6 (A′−H′) the same information is reported for cavity B.

From the analysis of cavity A, it results that its behavior is not affected by the adsorption on the electrode. Indeed, both for the monomeric and the dimeric system, the opening and closure of cavity A is well evident from the plot of the C_α distance (the only exception is for the monomeric oxidized ensemble in which the open state is poorly sampled). A deeper structural inspection of both the closed and the open conformation does not reveal any deformation of the cavity structure in all simulation ensembles with respect to the cavity observed in solution.

The analysis of cavity B reveals instead relevant differences with respect to the freely diffusing YCC. The cavity is indeed both structurally and dynamically different from the one observed in solution (a schematic representation of the deformed structure of cavity B when YCC is adsorbed on gold is provided in the Supporting Information). From a dynamic point of view, transitions between the open and the closed conformation (as previously defined) of the cavity are not seen in the plot of the C_α distance as a function of time. The C_α distance mainly oscillates around a value that, according to the previous definition, belongs to the closed conformation. The mobility of cavity B is thus mainly limited to a distorted closed conformation. This behavior seems to be ascribable to the presence of the electrode as, while cavity A is in the upper part of the protein (with respect to the gold surface) and fully exposed to the solvent, cavity B points to the gold surface (see Figure 6D,H,D′,H′). The steric hindrance of the electrode is likely to limit the fluctuations of the residues that are in its vicinity, preventing in the present case the natural reversible opening and closure of cavity B. This hypothesis is supported by the observation that in the dimeric system, as a consequence of the packing of the proteins on the surface, the distance between the cavity and the surface is higher than in the monomeric system (see the Supporting Information): the distribution of the C_α distance in the dimeric system is indeed broader and reaches higher values.

As previously mentioned, for the freely diffusing YCC the access of water to the propionates allowed by the opening of the cavities determines a rise of the redox potential of ≈45−50 mV. According to this, the different behavior of cavity B when YCC is adsorbed on gold could modify the hydration state of propionate 7 with possible effects on the redox potential. The analysis of the number of molecules residing in the first hydration shell of propionate 7 reveals instead that the observed distorted conformation of the cavity allows the access of water to the propionate (see the Supporting Information). According to the definition used for YCC freely diffusing in solution, when YCC is adsorbed on gold the cavity is neither fully open nor fully closed. However, the hydration of the propionate, which is at the basis of the changes observed in the redox potential in solution, is not affected by the different dynamic behavior of cavity B for YCC on gold.

Yet, it has to be remarked that the modification of the behavior of the cavity determined by the vicinity of the electrode could play a role in the electron transfer process between YCC and the gold surface. Indeed, as previously hypothesized for YCC in solution, the reversible opening of the cavities could act as a mechanism of fine-tuning of the redox potential to facilitate electron exchange events. In other words, the inhibition of the natural reversible opening of cavity B could interfere with transient adjustments of the reduction potential toward more negative values necessary to enhance the ET rate. Site-specific modifications, with the insertion of cysteines in the protein surface in order to bind the electrode with different orientations that prevent the deformation of the cavity, could improve the electron transfer kinetics with interesting technological fallout.

■ CONCLUSIONS

In the present work, a computational study of the thermodynamic, structural and dynamic properties of YCC adsorbed on a gold surface has been performed.

dx.doi.org/10.1021/ja505251a | J. Am. Chem. Soc. 2014, 136, 12929−12937

Using a hybrid quantum mechanics/molecular mechanics methodology, the perturbed matrix method, the redox potential of YCC bound to a gold electrode is calculated, reproducing the experimental conditions of an electrode with both low and high surface coverage. The computed values of the redox potentials are in very good agreement with the experimental ones and confirm the hypothesis that the crowding of the proteins on the gold surface affects the redox potential. Indeed, a high concentration of proteins on the electrode surface raises the redox potential of ≈100 mV. Such a rise has been demonstrated to depend on the polarizability of the environment that surrounds the protein rather than by a direct electrostatic potential effect: the monomeric system is fully surrounded by water, which is polarized upon oxidation of the protein; in the dimeric system, part of such water is replaced by a much less polarizable protein. This leads to a destabilization of the oxidized state and thus to a raise of the redox potential. Since environmental polarizability and exposure to water is known to play a crucial role in determining reorganization energy,[23,56,57] it is likely that also this quantity may be affected by the protein coverage.

The mechanisms here identified have remarkable analogies to some previously identified as peculiar of a crowded biochemical environment. Indeed, the presence of nearby proteins minimizes deformations of the protein with respect to the low concentration case. Similarly, in the usual biochemical context, crowding is deemed responsible for preventing some protein deformations, such as transition toward unfolded states.[58] Also, the main effect on the redox potential is due to a change in the polarizability of the environment surrounding the protein, due to the displacement of water realized by the other coadsorbed proteins. Again, crowding is known to change the property of a protein by replacing water in its surrounding with macromolecules.

The structural and dynamic features that characterize YCC adsorbed on a gold surface are also investigated and compared to the ones of YCC freely diffusing in solution. The secondary structure of the protein is substantially retained upon adsorption on the electrode. A relevant difference in the dynamic behavior of the protein is also noticed: in solution, two cavities in the protein surface were identified, whose reversible opening allows the access of water to the heme propionates inducing variations of the reduction potential.[32] The presence of the gold electrode was demonstrated to cause the deformation of one of these cavities and to inhibit its natural movement. Nevertheless, such a different behavior does not affect the hydration of the propionate and, therefore, the redox potential.

The thermodynamic, structural and dynamic analysis here performed not only clarifies the experimentally observed raise of the redox potential and explains its origin, but also highlights some relevant features that could affect the electron transfer process between the protein active site and the electrode.

■ ASSOCIATED CONTENT

Supporting Information

Additional analyses on the structural and dynamic behavior of YCC adsorbed on gold. This material is available free of charge via the Internet at http://pubs.acs.org/.

■ AUTHOR INFORMATION

Corresponding Authors

laura.zanettipolzi@nano.cnr.it

stefano.corni@nano.cnr.it

Notes

The authors declare no competing financial interest.

■ ACKNOWLEDGMENTS

The authors thank Andrea Amadei and Massimiliano Aschi for fruitful discussions and helpful comments. The authors acknowledge the CINECA award IsC11_PHOSPHO under the ISCRA initiative for the availability of high-performance computing resources and support. L.Z.P. and S.C. acknowledge funding from IIT through Seed Project MOPROSURF and Platform Computations and from MIUR through PRIN 2012A7LMS3 003.

■ REFERENCES

(1) Sarma, A. K.; Vatsyayan, P.; Goswami, P.; Minteer, S. D. *Biosens. Bioelectron.* **2009**, *24*, 2313−2322.
(2) Chen, C.; Xie, Q.; Yang, D.; Xiao, H.; Fu, Y.; Tana, Y.; Yao, S. *RSC Adv.* **2013**, *3*, 4473−4491.
(3) Chen, Y.-S.; Hong, M.-Y.; Huang, G. S. *Nat. Nanotechnol.* **2012**, *7*, 197−203.
(4) Willner, I.; Yan, Y.-M.; Willner, B.; Tel-Vered, R. *Fuel Cells* **2008**, *1*, 7−24.
(5) Ivanov, I.; Vidakovi-Koch, T.; Sundmacher, K. *Energies* **2010**, *3*, 803−846.
(6) Cracknell, J. A.; Vincent, K. A.; Armstrong, F. A. *Chem. Rev.* **2008**, *108*, 2439−2461.
(7) Alessandrini, A.; Corni, S.; Facci, P. *Phys. Chem. Chem. Phys.* **2006**, *8*, 4383−4397.
(8) Bortolotti, C. A.; Borsari, M.; Sola, M.; Chertkova, R.; Dolgikh, D.; Kotlyar, A.; Facci, P. *J. Phys. Chem. C* **2007**, *111*, 12100−12105.
(9) Amdursky, N.; Ferber, D.; Bortolotti, C. A.; Dolgikh, D. A.; Chertkova, R. V.; Pecht, I.; Sheves, M.; Cahen, D. *Proc. Natl. Acad. Sci. U. S. A.* **2014**, *111*, 5556−5561.
(10) Latour, R. A. *Biointerphases* **2008**, *3*, FC2−FC12.
(11) Bellucci, L.; Brancolini, G.; Calzolari, A.; Carrillo-Parramon, O.; Corni, S.; Di Felice, R. In *Proteins at Interfaces III State of the Art*; Horbett, T., Brash, J. L., Norde, W., Eds.; American Chemical Society: Washington, DC, 2012; Chapter 11, pp 229−250.
(12) Krishna, M. M. G.; Lin, Y.; Rumbley, J. N.; Englander, S. W. *J. Mol. Biol.* **2003**, *331*, 29−36.
(13) Kagan, V. E.; Tyurin, V. A.; Jiang, J.; Tyurina, Y. Y.; Ritov, V. B.; Amoscato, A. A.; Osipov, A. N.; Belikova, N. A.; Kapralov, A. A.; Kini, V.; Vlasova, I. I.; Zhao, Q.; Zou, M.; Di, P.; Svistunenko, D. A.; Kurnikov, I. V.; Borisenko, G. G. *Nat. Chem. Biol.* **2005**, *1*, 223−232.
(14) Maity, H.; Maity, M.; Krishna, M. M. G.; Mayne, L.; Englander, S. W. *Proc. Natl. Acad. Sci. U. S. A.* **2005**, *102*, 4741−4746.
(15) Sagle, L. B.; Zimmermann, J.; Matsuda, S.; Dawson, P. E.; Romesberg, F. E. *J. Am. Chem. Soc.* **2006**, *128*, 7909−7915.
(16) Jin, B.; Wang, G.-X.; Millo, D.; Hildebrandt, P.; Xia, X.-H. *J. Phys. Chem. C* **2012**, *116*, 13038−13044.
(17) Simonson, T.; Perahia, D. *J. Am. Chem. Soc.* **1995**, *117*, 7987−8000.
(18) Muegge, I.; Qi, P. X.; Wand, A. J.; Chu, Z. T.; Warshel, A. *J. Phys. Chem. B* **1997**, *101*, 825−836.
(19) Gorba, C.; Geyer, T.; Helms, V. *J. Chem. Phys.* **2004**, *121*, 457−464.
(20) Zhou, J.; Zheng, J.; Jiang, S. *J. Phys. Chem. B* **2004**, *108*, 17418−17424.
(21) DeBiase, P. M.; Alvarez-Paggi, D.; Doctorovich, F.; Hildebrandt, P.; Estrin, D. A.; Murgida, D. H.; Marti, M. A. *J. Am. Chem. Soc.* **2009**, *131*, 16248−16256.
(22) Alvarez-Paggi, D.; Martin, D. F.; DeBiase, P. M.; Hildebrandt, P.; Marti, M. A.; Murgida, D. H. *J. Am. Chem. Soc.* **2010**, *132*, 5769−5778.
(23) Bortolotti, C. A.; Siwko, M. E.; Castellini, E.; Ranieri, A.; Sola, M.; Corni, S. *J. Phys. Chem. Lett.* **2011**, *2*, 1761−1765.

(24) Bortolotti, C. A.; Battistuzzi, G.; Borsari, M.; Facci, P.; Ranieri, A.; Sola, M. *J. Am. Chem. Soc.* **2006**, *128*, 5444−5451.
(25) Heering, H. A.; Wiertz, F. G. M.; Dekker, C.; deVries, S. *J. Am. Chem. Soc.* **2004**, *126*, 11103−11112.
(26) Siwko, M. E.; Corni, S. *Phys. Chem. Chem. Phys.* **2013**, *15*, 5945−5956.
(27) Gao, J.; Truhlar, D. G. *Annu. Rev. Phys. Chem.* **2002**, *53*, 467−505.
(28) Meier, K.; Thiel, W.; van Gunsteren, W. F. *J. Comput. Chem.* **2012**, *33*, 363−378.
(29) Aschi, M.; D'Abramo, M.; Ramondo, F.; Daidone, I.; D'Alessandro, M.; Di Nola, A.; Amadei, A. *J. Phys. Org. Chem.* **2006**, *19*, 518−530.
(30) Zanetti-Polzi, L.; Amadei, A.; Aschi, M.; Daidone, I. *J. Am. Chem. Soc.* **2011**, *133*, 11414−11417.
(31) Daidone, I.; Amadei, A.; Zaccanti, F.; Borsari, M.; Bortolotti, C. A. *J. Phys. Chem. Lett.* **2014**, *5*, 1534−1540.
(32) Bortolotti, C. A.; Amadei, A.; Aschi, M.; Borsari, M.; Corni, S.; Sola, M.; Daidone, I. *J. Am. Chem. Soc.* **2012**, *134*, 13670−13678.
(33) van Gunsteren, W. F.; Billeter, S.; Eising, A.; Hunenberg, P.; Kruger, P.; Mark, A. E.; Scott, W.; Tironi, I. *Biomolecular Simulations: The GROMOS96 Manual and User Guide*; Hochschulverlag an der ETH Zurich: Zurich, 1996.
(34) Iori, F.; Di Felice, R.; Molinari, E.; Corni, S. *J. Comput. Chem.* **2009**, *30*, 1465−1476.
(35) Iori, F.; Corni, S. *J. Comput. Chem.* **2008**, *29*, 1656−1666.
(36) Brosseau, C. L.; Roscoe, S. G. *Electrochim. Acta* **2006**, *51*, 2145−2152.
(37) Berendsen, H. J. C.; Grigera, J. R.; Straatsma, T. P. *J. Phys. Chem.* **1987**, *91*, 6269−6271.
(38) Hoefling, M.; Iori, F.; Corni, S.; Gottschalk, K.-E. *Langmuir* **2010**, *26*, 8347−8351.
(39) Brown, D.; Clarke, J. H. R. *Mol. Phys.* **1984**, *51*, 1243−1252.
(40) Darden, T.; York, D.; Pedersen, L. *J. Chem. Phys.* **1993**, *98*, 10089−10092.
(41) Hess, B.; Bekker, H.; Berendsen, H. J. C.; Fraaije, J. G. E. M. *J. Comput. Chem.* **1997**, *18*, 1463−1472.
(42) Berendsen, H. J. C.; van der Spoel, D.; van Drunen, R. *Comput. Phys. Commun.* **1995**, *91*, 43−56.
(43) Hay, P. J.; Wadt, W. R. *J. Chem. Phys.* **1985**, *82*, 299−310.
(44) Krishnan, R.; Binkley, J. S.; Seeger, R.; Pople, J. A. *J. Chem. Phys.* **1980**, *72*, 650−654.
(45) Aschi, M.; Zazza, C.; Spezia, R.; Bossa, C.; Di Nola, A.; Paci, M.; Amadei, A. *J. Comput. Chem.* **2004**, *25*, 974−984.
(46) Frisch, M. J.; et al. *Gaussian 03*, Revision C.02; Gaussian Inc.: Wallingford, CT, 2004.
(47) Aschi, M.; Spezia, R.; Di Nola, A.; Amadei, A. *Chem. Phys. Lett.* **2001**, *344*, 374−380.
(48) Spezia, R.; Aschi, M.; Di Nola, A.; Amadei, A. *Chem. Phys. Lett.* **2002**, *365*, 450−456.
(49) Amadei, A.; D'Abramo, M.; Zazza, C.; Aschi, M. *Chem. Phys. Lett.* **2003**, *381*, 187−193.
(50) Amadei, A.; Marinelli, F.; D'Abramo, M.; D'Alessandro, M.; Anselmi, M.; Di Nola, A.; Aschi, M. *J. Chem. Phys.* **2005**, *122*, 124506.
(51) Amadei, A.; D'Alessandro, M.; D'Abramo, M.; Aschi, M. *J. Chem. Phys.* **2009**, *130*, 08410−08415.
(52) Vreven, T.; Morokuma, K. *Annu. Rep. Comput. Chem.* **2006**, *2*, 35−51.
(53) Senn, H. M.; Thiel, W. *Curr. Opin. Chem. Biol.* **2007**, *11*, 182−187.
(54) Amadei, A.; D'Alessandro, M.; Aschi, M. *J. Phys. Chem. B* **2004**, *108*, 16250−16254.
(55) Marracino, P.; Apollonio, F.; Liberti, M.; d'Inzeo, G.; Amadei, A. *J. Phys. Chem. B* **2013**, *117*, 2273−2279.
(56) Kornyshev, A. A.; Kuznetsov, A. M.; Ulstrup, J.; Stimming, U. *J. Phys. Chem. B* **1997**, *101*, 5917−5935.
(57) Corni, S. *J. Phys. Chem. B* **2005**, *109*, 3423−3430.
(58) Yuan, J.-M.; Chyan, C.-L.; Zhou, H.-X.; Chung, T.-Y.; Peng, H.; Ping, G.; Yang, G. *Protein Sci.* **2008**, *17*, 2156−2166.